Atmos. Chem. Phys. Discuss., doi:10.5194/acp-2017-58, 2017
Manuscript under review for journal Atmos. Chem. Phys.
Discussion started: 8 February 2017

Atmospheric Chemistry and Physics Discussions

Experimental determination of Henry's law constants of difluoromethane (HFC-32) and the salting-out effects in aqueous salt solutions relevant to seawater

Shuzo Kutsuna

National Institute of Advanced Industrial Science and Technology (AIST), 16-1 Onogawa, Tsukuba, 305-8569, Japan

Correspondence to: S. Kutsuna (s-kutsuna@aist.go.jp)

Abstract. Gas-to-water equilibrium coefficients, K_{eq}^{S} (in M atm^{-1}) of difluoromethane (CH_2F_2), a hydrofluorocarbon refrigerant (HFC-32), in aqueous salt solutions relevant to seawater were determined over a temperature (T) range from 276 to 313 K and a salinity (S) range up to 51 ‰ by means of an inert-gas stripping method. From the van't Hoff equation, the K_{eq}^{S} value in water, which corresponds to the Henry's law constant (K_H), at 298 K was determined to be 0.064 M atm^{-1}. The salinity dependence of K_{eq}^{S} (the salting-out effect), $\ln(K_H/K_{eq}^{S})$, did not obey the Sechenov equation but was represented by an equation involving S and $S^{0.5}$. Overall, the $K_{eq}^{S}(T)$ value was expressed by $\ln(K_{eq}^{S}(T)) = -49.7122 + 77.7018\times(100/T) + 19.1379\times\ln(T/100) + [-0.2261 + 0.5176\times(T/100)] \times S^{0.5} + [0.0362 - 0.1046\times(T/100)] \times S$. By using this equation in a lower tropospheric semi-hemisphere (30° S–90° S) of the Advanced Global Atmospheric Gases Experiment (AGAGE) 12-box model, we estimated that 1 to 5 % of the atmospheric burden of CH_2F_2 resided in the ocean mixed layer and that this percentage was at least 5 % in the winter; dissolution of CH_2F_2 in the ocean may partially influence estimates of CH_2F_2 emissions from long-term observational data of atmospheric CH_2F_2 concentrations.

1 Introduction

Hydrofluorocarbons (HFCs) have been developed as replacements for chlorofluorocarbons and hydrochlorofluorocarbons (HCFCs) to protect the stratospheric ozone layer from depletion. In particular, difluoromethane (HFC-32, CH_2F_2) has been used as a refrigerant to replace HCFC-22 ($CHClF_2$): azeotropic mixtures of CH_2F_2 with HFC-125 (CHF_2CF_3) and HFC-134a (CH_2FCF_3) have been used as refrigerants for air conditioning and refrigeration for a few decades, and CH_2F_2 alone has recently been used as a refrigerant for air conditioning.

However, HFCs can act as greenhouse gases, and thus there is concern about emissions of CH_2F_2 and other HFCs to the atmosphere, where they can accumulate and contribute to global warming (IPCC, 2013). Observational data from the Advanced Global Atmospheric Gases Experiment (AGAGE) indicate that the atmospheric concentration of CH_2F_2 has been increasing every year since 2004; in 2012, the global mean mole fraction of CH_2F_2 was 6.2 ± 0.2 parts per trillion (ppt), and the rate of increase was 1.1 ± 0.04 ppt y^{-1} (17% y^{-1}) (O'Doherty et al., 2014). By using AGAGE data in combination with a chemical transport model such as the AGAGE 12-box model (Cunnold et al., 1994; Rigby et al., 2013) and a value of 5.1

Atmos. Chem. Phys. Discuss., doi:10.5194/acp-2017-58, 2017
Manuscript under review for journal Atmos. Chem. Phys.
Discussion started: 8 February 2017

Atmospheric Chemistry and Physics Discussions

years as the atmospheric lifetime of CH_2F_2, O'Doherty et al. (2014) estimated the global emission rate of CH_2F_2 in 2012 to be 21 ± 11 Gg y^{-1} with an increase rate of 14 ± 11% y^{-1}. Such estimates on the basis of long-term observational data such as the AGAGE and the National Oceanic and Atmospheric Administration Global Monitoring Division (NOAA GMD) network are called top-down estimates and have been shown to provide an independent and effective method for assessing the accuracy of globally and regionally aggregated reductions or increases in emissions of individual HFCs, as well as other greenhouse gases, compiled from national reports to the United Nations Framework Convention on Climate Change (eg. Prinn et al., 2000; Lunt et al., 2015; Montzka et al., 2015).

The atmospheric lifetimes of HFCs are thus related to their estimated emission rates. The currently accepted value of the atmospheric lifetime of CH_2F_2, which was revised in 2014 (Carpenter et al., 2014), is 5.4 years. The partial atmospheric lifetime of CH_2F_2 with respect to gas-phase reactions with OH in the troposphere is 5.5 years, and that with respect to stratospheric removal processes is 124 years. Other processes, such as dissolution into seawater, are not considered to contribute significantly to atmospheric removal of CH_2F_2. Yvon-Lewis and Butler (2002) estimated partial atmospheric lifetimes of some HCFCs and HFCs with respect to irreversible dissolution into seawater by using physicochemical properties such as solubility and aqueous reaction rates, as well as meteorological data such as temperature and wind speed over the ocean in grids. Their estimates indicated that dissolution into seawater is not a significant sink of the HCFCs and HFCs that were evaluated in the study. Because no aqueous reactions of CH_2F_2 have yet been observed under environmental conditions, dissolution of CH_2F_2 into seawater is considered to be reversible and cannot serve as a sink of CH_2F_2. However, because CH_2F_2 is more soluble in water than HCFCs and other HFCs (Sander, 2015), even reversible dissolution of CH_2F_2 into seawater might influence a top-down estimate of CH_2F_2 emission rates.

The objective of the present study is to experimentally determine the seawater solubility of CH_2F_2, which is a physicochemical property necessary for estimating the residence ratio of CH_2F_2 in the ocean when the ocean mixed layer is at solubility equilibrium with the atmosphere. Specifically, the Henry's law constants, K_H (in M atm^{-1}), of CH_2F_2 and the salting-out effects of seawater-relevant ions on CH_2F_2 solubility were experimentally determined. Values of K_H for CH_2F_2 have been reported in some review papers (Sander, 2015; Clever et al., 2005). The largest and smallest values at 298K differ from each other by a factor of approximately 3: 0.87 M atm^{-1} (Sander, 2015; Yaws and Yang, 1992) and 0.30 M atm^{-1} (Clever et al., 2005; Miguel et al., 2000). To the author's knowledge, no data on the salting-out effects of seawater-relevant ions on CH_2F_2 solubility have been reported.

First, the values of K_H for CH_2F_2 were first determined over the temperature range from 276 to 313 K by means of an inert-gas stripping (IGS) method. The K_H values were also determined over the temperature range from 313 to 353 K by means of a phase ratio variation headspace (PRV-HS) method. The K_H values obtained by the two methods could be fitted by an equation representing the same temperature dependence. Second, salting-out effects on CH_2F_2 solubility were determined over the temperature range from 276 to 313 K for test solutions of artificial seawater prepared over the salinity range from 4.5 to 51.5 ‰. The salting-out effects were confirmed for the artificial seawater, but the relationship between CH_2F_2 solubility and salinity of the artificial seawater was found to be unusual in that the excessive free energy for dissolution was

Atmos. Chem. Phys. Discuss., doi:10.5194/acp-2017-58, 2017
Manuscript under review for journal Atmos. Chem. Phys.
Discussion started: 8 February 2017

not proportional to the salinity but rather was represented by an equation involving the salinity and the 0.5 power of the salinity. Over the salinity range relevant to seawater, the solubility of CH_2F_2 in the artificial seawater could be represented as a function of both salinity and temperature. Third, on the basis of the solubility of CH_2F_2 in seawater determined in this study and a global gridded dataset of monthly mean values of temperature, salinity, and depth of the ocean mixed layer, the amounts of CH_2F_2 dissolved in the ocean mixed layer were estimated in each month for each lower tropospheric semi-hemisphere of the AGAGE-12 box model.

2 Experimental

2.1 Materials

CH_2F_2 gas (1010 ppmv or 1000 ppmv in synthetic air) was purchased from Takachiho Chemical Industrial Co. (Tokyo, Japan). Sodium chloride (NaCl, >99.5%), sodium sulfate (Na_2SO_4, >99%), magnesium chloride ($MgCl_2 \cdot 6H_2O$, >98%), calcium chloride ($CaCl_2 \cdot 2H_2O$, >99.9%), and potassium chloride (KCl, >99.5%) were purchased from Wako Pure Chemical Industries (Osaka, Japan) and used as supplied. Water was purified with a Milli-Q Gradient A10 system (>18 MΩ).

Synthetic artificial seawater was prepared as described by Platford (1965) and was used to evaluate the salting-out effects on the solubility of CH_2F_2 in the ocean. The prepared artificial seawater had the following definite mole ratios: 0.4240 NaCl, 0.0553 $MgCl_2$, 0.0291 Na_2SO_4, 0.0105 $CaCl_2$, and 0.0094 KCl. The ionic strength of the artificial seawater was set between 0.089 and 1.026 mol kg^{-1} water, that is, at molality base, with each salt at the aforementioned mole ratio; the salinity (in ‰) of this artificial seawater was between 4.45 and 51.53‰. This artificial seawater is referred to hereafter as a-seawater.

2.2 Inert-gas stripping method with a helical plate

An inert-gas stripping (IGS) method (Mackay et al., 1979) was used to determine the solubility of CH_2F_2 in water and aqueous salt solutions. A CH_2F_2–air-nitrogen mixture (mixing ratio of $CH_2F_2 \sim 10^{-4}$) was bubbled into the aqueous solution for a certain time period (e.g., 5 min), and then nitrogen gas (N_2) was bubbled through the resulting aqueous solution containing CH_2F_2, which was stripped from the solution into the gas phase.

The gas-to-liquid partition coefficient (in M atm^{-1}) at temperature T (in K), $K_{eq}(T)$, was calculated from the rate of decrease of the gas-phase partial pressure according to Eqs. (1) and (2):

$$\ln(P_t/P_0) = -k_1 t \quad (1)$$

$$k_1 = \frac{1}{K_{eq}(T)RT}\frac{F}{V} \quad (2)$$

where P_t/P_0 is the ratio of the partial pressure of CH_2F_2 at time t to the partial pressure of CH_2F_2 at fixed time t_0; k_1 is the first-order decreasing rate constant (in s^{-1}); F is the flow rate of N_2 (in $dm^3\ s^{-1}$); V is the volume of water or aqueous salt

Atmos. Chem. Phys. Discuss., doi:10.5194/acp-2017-58, 2017
Manuscript under review for journal Atmos. Chem. Phys.
Discussion started: 8 February 2017

Atmospheric Chemistry and Physics Discussions

solution (in dm^3); and R is the gas constant (0.0821 dm^3 atm K^{-1} mol^{-1}). The $K_{eq}(T)$ values in water correspond to the Henry's law constants, $K_H(T)$ in M atm^{-1}. The P_t values typically ranged from 10^{-4} to 10^{-6} atm.

A stripping column apparatus with a helical plate was used to strip CH_2F_2. This apparatus was described in detail by Kutsuna and Hori (2008) and is described briefly here. The stripping column consisted of a jacketed Duran glass column (4 cm i.d. × 40 cm height) and a glass gas-introduction tube with a glass helix. Water or a-seawater (0.300 or 0.350 dm^3) was added to the column for the test solution. The solution was magnetically stirred, and its temperature was kept constant by means of a constant-temperature bath that had both heating and cooling capabilities (NCB-2500, EYELA, Tokyo, Japan) and was connected to the water jacket of the column.

Experiments were conducted at nine temperatures in the range of 276 to 313 K. A CH_2F_2–air mixture or N_2 was introduced near the bottom of the column through a hole (~1 mm in diameter) in the gas-introduction tube. The bubbles travelled along the underside of the glass helix from the bottom to the top of the column, at which point they entered the headspace of the column. The gas flow was controlled by means of calibrated mass flow controllers (M100 Series, MKS Japan, Inc., Tokyo, Japan) and was varied between 2.2×10^{-4} and 4.4×10^{-4} dm^3 s^{-1} (STP).

The volumetric flow rate of the gas (F_{meas}) was calibrated with a soap-bubble meter for each experimental run. The soap-bubble meter had been calibrated by means of a high-precision film flow meter SF-1U with VP-2U (Horiba, Kyoto, Japan). To prevent water evaporation from the stripping column, the gas was humidified prior to entering the stripping column passage through a vessel containing deionized water. This vessel was immersed in a water bath at the same temperature as the stripping column. All volumetric gas flows were corrected to prevailing temperature and pressure by Eq. (3) (Krummen et al., 2000).

$$F = F_{meas} \times \frac{P_{meas} - h_{meas}}{P_{hs} - h} \times \frac{T}{T_{meas}} \quad (3),$$

where P_{meas} and T_{meas} are the ambient pressure and temperature, respectively, at which F_{meas} was calibrated; P_{hs} is the headspace total pressure over the test solution in an IGS method experiment with a flow rate of F at temperature of T; and h_{meas} is the saturated vapour pressure, in atm, of water at T_{meas}; h is the saturated vapor pressure, in atm, of water or a-seawater at T. Values of h_{meas} and h were calculated by use of Eq. (4) where S is salinity of a-seawater (Weiss and Price, 1980).

$$h \text{ or } h_{meas} = \exp\left[24.4543 - 67.4509 \times \left(\frac{100}{T}\right) - 4.8489 \times \ln\left(\frac{T}{100}\right) - 0.000544 \times S\right] \quad (4)$$

The purge gas flow exiting from the stripping column was diluted with constant flow of N_2 to prevent water vapour from condensing. The CH_2F_2 in the purge gas flow thus diluted was determined by means of gas chromatography–mass spectrometry (GC-MS) on an Agilent GC6890N with 5973inert instrument (Agilent Technologies, Palo Alto, CA). A portion of the purge gas containing CH_2F_2 stripped from the test solution was injected into the GC-MS instrument in split mode (split ratio = 1:30) with a six-port sampling valve (VICI AG, Valco International, Schenkon, Switzerland) equipped with a stainless sampling loop (1.0 cm^3). Gas was sampled automatically at intervals of 10 to 11 min during an experimental run

Atmos. Chem. Phys. Discuss., doi:10.5194/acp-2017-58, 2017
Manuscript under review for journal Atmos. Chem. Phys.
Discussion started: 8 February 2017

(which lasted from 2 to 8 h), depending on the decay rate of the partial pressure of CH_2F_2. Peaks due to CH_2F_2 were measured in selected-ion mode (m/z = 33, CH_2F^+). A PoraBOND-Q capillary column (0.32-mm i.d. × 50-m length, Agilent Technologies) was used to separate CH_2F_2. The column temperature was kept at 308 K. Helium was used as the carrier gas. The injection port was kept at 383 K.

If CH_2F_2 in the headspace over the test solution is redistributed into the test solution, k_1 should be represented by Eq. (5) instead of Eq. (2) (Krummen et al., 2000; Brockbank et al., 2013).

$$k_1 = \frac{F}{K_{\mathrm{eq}}(T)RTV + V_{\mathrm{head}}} \quad (5),$$

where V_{head} is headspace volume over the test solution. In this study, the values of V_{head} were 0.070 and 0.020 dm^3 for V values of 0.300 and 0.350 dm^3, respectively. Equations (6) and (7) are derived from Eqs. (2) and (5), respectively:

$$K_{\mathrm{eq}}(T) = \frac{1}{k_1 RT}\frac{F}{V} \quad (6),$$

$$K_{\mathrm{eq}}(T) = \frac{1}{k_1 RT}\frac{F}{V} - \frac{V_{\mathrm{head}}}{RTV} \quad (7).$$

As described in *Results and discussion* (Sect. 3.1), CH_2F_2 in the headspace over the test solution was not expected to be redistributed into the test solution. Hence Eq. (6) was used to deduce $K_{\mathrm{eq}}(T)$ from k_1.

2.3 Phase ratio variation headspace method

The K_{H} values of CH_2F_2 in water were also determined by means of the phase ratio variation headspace (PRV-HS) method (Ettre et al., 1993) for comparison with the results obtained by the above-described IGS method. The PRV-HS method experiments were performed over the temperature range from 313 to 353 K at 10 K intervals because the headspace temperature in the equipment used here could not be controlled at less than 313 K. The experimental procedure was the same as that described in detail previously (Kutsuna, 2013) and it is described briefly here.

The determination was carried out by GC-MS on an Agilent GC6890N with 5973inert instrument (Agilent Technologies) equipped with an automatic headspace sampler (HP7694, Agilent Technologies). The headspace samples were slowly and continuously shaken by a mechanical set-up for the headspace equilibration time (1 h; see below), and then the headspace gas (1 cm^3) was injected into the gas chromatograph in split mode (split ratio = 1:30). The conditions used for GC-MS were the same as those described in Sect. 2.2.

Headspace samples containing five different amounts of CH_2F_2 and six different volumes of water were prepared for an experimental run at each temperature as follows (30 samples total). Volumes (V_i) of 1.5, 3.0, 4.5, 6.0, 7.5, and 9.0 cm^3 of deionized water were pipetted into six headspace vials with a total volume (V_0) of 21.4 cm^3 (V_i/V_0 = 0.070, 0.140, 0.210, 0.280, 0.350, and 0.421, respectively). Five sets of six headspace vials were prepared and sealed. A prescribed volume (v_j) of a standard gas mixture of CH_2F_2 and air was added to each set of five vials containing the same volume (V_i) of water by

Atmos. Chem. Phys. Discuss., doi:10.5194/acp-2017-58, 2017
Manuscript under review for journal Atmos. Chem. Phys.
Discussion started: 8 February 2017

Atmospheric Chemistry and Physics Discussions

means of a gas-tight syringe (v_j = 0.05, 0.10, 0.15, 0.20, or 0.25 cm^3). The headspace partial pressure of CH_2F_2 thus prepared ranged from 10^{-5} to 10^{-6} atm.

The time required for equilibration between the headspace and the aqueous solution was determined by analyzing the headspaces over the test samples as a function of time until steady-state conditions were attained. In Fig. S1, the relative signal intensities of the GC-MS peaks for CH_2F_2, that is, the ratio of the headspace partial pressure at time t to that at 60 min (P_t/P_{60}), are plotted against the time (t_h) during which samples were placed in the headspace oven. The plot shows that the peak area did not change after 60 min (Fig. S1). Therefore, the headspace equilibration time was set at 1 h for all the measurements.

If P_{ij} is the equilibrium partial pressure (in atm) of a CH_2F_2 sample in a vial with volume V_0 (in cm^3) containing a volume V_i (in cm^3) of water and a volume v_j (in cm^3) of a CH_2F_2 gas mixture, and if P_j is the equilibrium partial pressure (in atm) of CH_2F_2 in a sample containing volume v_j (in cm^3) of a CH_2F_2 gas mixture without water, then Eq. (8) applies:

$$\frac{P_j V_0}{RT} = K_{\mathrm{eq}}(T) P_{ij} V_i + \frac{P_{ij}(V_0 - V_i)}{RT} \tag{8}$$

Because the signal peak area of CH_2F_2 (S_{ij}) at partial pressure P_{ij} is expected to be proportional to v_j for each set of samples with the same V_i, a plot of S_{ij} versus v_j should be a straight line that intercepts the origin:

$$S_{ij} = L_i v_j \tag{9}$$

The slope of the line, L_i, corresponds to S_{ij} at v_j = 1.0 cm^3. If L is the slope corresponding to P_i at V_i = 0, then

$$\frac{1}{L_i} = \frac{1}{L} + \frac{RTK_{\mathrm{eq}}(T) - 1}{L} \frac{V_i}{V_0} \tag{10}$$

Plotting $1/L_i$ against V_i/V_0 gives an intercept of $1/L$ and a slope of $[RT\,K_{\mathrm{eq}}(T) - 1]/L$, and $K_{\mathrm{eq}}(T)$ can be obtained from these two values. Therefore, $K_{\mathrm{eq}}(T)$ can be determined by recording the peak area S_{ij}, deriving L_i from a plot of S_{ij} versus v_j, and then applying regression analysis to plots of $1/L_i$ versus V_i/V_0 with respect to Eq. (10).

Furthermore, values of $K_{\mathrm{eq}}(T)$ and errors of them were determiend by non-liner fitting of the data of L_i and V_i/V by means of Eq. (11), which was obtained from Eq. (10):

$$L_i = \frac{L}{1 + (RTK_{\mathrm{eq}}(T) - 1)\frac{V_i}{V_0}} \tag{11}$$

3 Results and discussion

3.1 Determination of Henry's law constants

In the IGS method experiment, an aqueous solution was purged with N_2 to strip CH_2F_2 from the solution into the N_2 purge gas flow, and the partial pressure of CH_2F_2 (P_t) in the N_2 purge gas flow decreased with time. Typically it took 20–100 min, depending on the purge gas flow rate and the temperature of the solution, for the decrease to show a first-order time profile. From the first-order time profile of P_t for the following period of 2–7 h, during which P_t typically decreased by 2

Atmos. Chem. Phys. Discuss., doi:10.5194/acp-2017-58, 2017
Manuscript under review for journal Atmos. Chem. Phys.
Discussion started: 8 February 2017

orders of magnitude, the first-order decreasing rate constant, k_1, was calculated according to Eq. (1). Values of k_1 were obtained at different volumes of deionized water (V), various purge gas flow rate (F), and various temperatures. Figure S2 shows an example of time profile of P_t and how to calculate the k_1 value.

Figure 1 plots values of $F/(k_1RTV)$, the right side of Eq. 6, against F for V values of 0.350 dm^3 and 0.300 dm^3 at each temperature T (K). Table 1 lists the average values of $F/(k_1RTV)$ for V values of 0.350 and 0.300 dm^3 at each temperature. Some data were excluded for calculation of the average so that the remaining data were inside the 2σ range; the data points thus excluded was only for V values of 0.350 dm^3 and the number of them were six or fewer at each temperature.

As is apparent in Fig. 1 and Table 1, the $F/(k_1RTV)$ values for the two V values (0.350 and 0.300 dm^3) agreed at each temperature. This agreement strongly suggests that $K_{eq}(T)$ is represented by Eq. (6) rather than by Eq. (7) because, if Eq. (7) were applicable, the $K_{eq}(T)$ values calculated for the V value of 0.300 dm^3 would be inconsistent with those for the V value of 0.350 dm^3: the former would be smaller than the latter by 0.007–0.008 M atm^{-1}. Redistribution of CH_2F_2 between the headspace and the test solution was probably negligible under the experimental conditions here; hence, values of $K_{eq}(T)$ should be calculated from Eq. (6) rather than Eq. (7).

The above-mentioned agreement also supports the idea that gas-to-water partitioning equilibrium of CH_2F_2 was achieved under the experimental conditions used for the IGS method. As described later, the achievement of gas-to-water partitioning equilibrium was also supported by comparison of these data with $K_{eq}(T)$ values obtained by the PRV-HS method. Hereafter only values of $F/(k_1RTV)$ for the V value of 0.350 dm^3 are used to deduce $K_{eq}(T)$ values. Because the $K_{eq}(T)$ values in water correspond to the Henry's law constants, $K_H(T)$ in M atm^{-1}, $K_H(T)$ is used instead of $K_{eq}(T)$ in this section.

Figure 2 plots the average K_H values for the V value of 0.350 dm^3 against $100/T$. Figure 2 also displays the $K_H(T)$ values obtained by the PRV-HS method. The results of the PRV-HS experiments are described in *Supporting Information* (Fig. S3, Fig. S4 and Table S1). The K_H value obtained by the PRV-HS experiments at each temperature and its error were estimated at 95% confidence level by fitting the two datasets at each temperature (Fig. S4) simultaneously by means of the nonlinear least-squares method with respect to Eq. (11).

All the K_H values were regressed with respect to the van't Hoff equation (Eq. (12)) (Clarke and Glew, 1965; Weiss, 1970):

$$K_H(T) = \exp\left(a_1 + a_2 \times \left(\frac{100}{T}\right) + a_3 \times \ln\left(\frac{T}{100}\right)\right) \quad (12).$$

The regression with respect to Eq. (12) gave Eq. (13).

$$\ln\left(K_H(T)\right) = -49.7122 + 77.7018 \times \left(\frac{100}{T}\right) + 19.1379 \times \ln\left(\frac{T}{100}\right) \quad (13).$$

In Fig. 2, the solid curve was obtained by Eq. (13). The $K_H(T)$ values calculated by Eq. (13) are listed in Table 1. Equation (13) can reproduce the average of K_H values at each temperature within an error of 5%. The dashed lines in Fig. 2 represent 95% confidence limits of the regression for fitting the $K_H(T)$ values by Eq. (12). Taking into consideration errors of the K_H

Atmos. Chem. Phys. Discuss., doi:10.5194/acp-2017-58, 2017
Manuscript under review for journal Atmos. Chem. Phys.
Discussion started: 8 February 2017

Atmospheric Chemistry and Physics Discussions

values, the K_H values obtained by the two methods were within the 95% confidence limits of the regression by Eq. (12); this result supports the idea that the values determined by the IGS method and the PRV-HS method were accurate.

The Gibbs free energy for dissolution of CH_2F_2 into water at temperature T ($\Delta G_{sol}(T)$) and the enthalpy for dissolution of CH_2F_2 into water (ΔH_{sol}) can be deduced from $K_H(T)$ by means of Eqs. (14) and (15):

$$\Delta G_{sol}(T) = \mu_l^{\circ}(T) - \mu_g^{\circ}(T) = -RT\ln(K_H(T)) \quad (14)$$

$$\Delta H_{sol}(T) = -R\frac{\partial[\ln(K_H(T))]}{\partial(1/T)} \quad (15)$$

where $\mu_l^{\circ}(T)$ is the chemical potential of CH_2F_2 under the standard-state conditions at a concentration of 1 M in aqueous solutions at temperature T; and $\mu_g^{\circ}(T)$ is the chemical potential of CH_2F_2 under the standard-state conditions at 1 atm of partial pressure in the gas phase at temperature T. The $K_H(T)$ and $\Delta H_{sol}(T)$ values at 298.15 K were calculated by means of Eqs. (13) and (15) and are listed in Table 2. $K_H(298.15)$ is represented by K_H^{298} hereafter.

Table 2 also lists literature values of K_H^{298} and ΔH_{sol} at 298.15 K for CH_2F_2 reported in two reviews (Clever et al., 2005; Sander, 2015) and by Anderson (2011); the units of the literature data were converted to M atm^{-1} for K_H^{298} and kJ mol^{-1} for ΔH_{sol}. The K_H^{298} value determined in this study was 7−9% smaller than the values reported by Maaβen (1995), Reichl (1995) and Anderson (2011), whereas the value reported by Yaws and Yang (1992), that reported by Hilal et al. (2008) and that reported by Miguel et al. (2000) were 1.3, 1.4 and 0.47 times, respectively, as large as the value determined here. The absolute value of ΔH_{sol} at 298.15 K determined here was by 1.4−3.4 kJ mol^{-1} less than the values determined by Maaβen (1995), Reichl (1995), Kühne et al. (2005) and Anderson (2011), whereas it was by 10 kJ mol^{-1} less than the value reported by Miguel et al. (2000).

3.2 Determination of salting-out effects in artificial seawater

The solubility of CH_2F_2 in a-seawater (Sect. 2.1) was determined by means of the IGS method (Sect. 2.2). According to Eq. (6), the $K_{eq}(T)$ values at an a-seawater salinity of S in ‰ were obtained by averaging the $F/(k_1RTV)$ values for the V value of 0.350 dm^3 at each salinity and temperature in a similar way as described in Sect. 3.1. Figure 3 plots values of $F/(k_1RTV)$ at each temperature against F for V values of 0.350 dm^3 at an a-seawater salinity of 36.074‰. Figures S5-S8 represent such plots at an a-seawater salinity of 4.452, 8.921, 21.520 and 51.534 ‰. The $K_{eq}(T)$ value at an a-seawater salinity of S in ‰ is represented by $K_{eq}^S(T)$ hereafter. Table 3 lists the $K_{eq}^S(T)$ values.

Figure 4 plots the $K_{eq}^S(T)$ values against $100/T$. The plots indicate a clear salting-out effect on CH_2F_2 solubility in a-seawater: that is, the solubility of CH_2F_2 in a-seawater decreased with increasing a-seawater salinity. For example, the solubility of CH_2F_2 in a-seawater at a salinity of 36.074‰ was 0.73–0.79 times the solubility in water at 3.0 to 39.5 °C.

In general, the salting-out effect on nonelectrolyte solubility in an aqueous salt solution of ionic strength I can be determined empirically by means of the Sechenov equation:

$$\ln(K_H(T)/K_{eq}^I(T)) = k_I I \quad (16)$$

Atmos. Chem. Phys. Discuss., doi:10.5194/acp-2017-58, 2017
Manuscript under review for journal Atmos. Chem. Phys.
Discussion started: 8 February 2017

Atmospheric Chemistry and Physics Discussions

where $K_{eq}^{I}(T)$ is the $K_{eq}(T)$ at ionic strength I in mol kg^{-1}; and k_I is the Sechenov coefficient for the molality- and natural logarithm-based Sechenov equation and is independent of I (Clegg and Whitfield, 1991). For a-seawater, a similar relationship between $K_{eq}^{S}(T)$ and S is expected:

$$\ln(K_H(T)/K_{eq}^{S}(T)) = k_S S \quad (17)$$

where k_S is the Sechenov coefficient for the salinity- and natural logarithm-based Sechenov equation and is independent of S. Figure 5 plots $\ln(K_H(T)/K_{eq}^{S}(T))$ against S at each temperature. If the $K_{eq}^{S}(T)$ values obeyed Eq. (17), the data at each temperature in Fig. 5 would fall on a straight line passing through the origin, but they did not. Figure 5 reveals that the salinity dependence of CH_2F_2 solubility in a-seawater cannot be represented by Eq. (17).

When the same data were plotted on a log–log graph (Fig. S9), a line with a slope of about 0.5 was obtained by linear regression. This result suggests that $\ln(K_H(T)/K_{eq}^{S}(T))$ varied according to Eq. (18):

$$\ln(K_H(T)/K_{eq}^{S}(T)) = k_{s1} S^{0.5} + k_{s2} S \quad (18)$$

Values of k_{s1} and k_{s2} may be represented by the following functions of T:

$$k_{s1} = a_1 + a_2 \times (100/T) \quad (19)$$

$$k_{s2} = a_3 + a_4 \times (100/T) \quad (20)$$

Parameterizations of a_1, a_2, a_3 and a_4 obtained by fitting all the $\ln(K_H(T)/K_{eq}^{S}(T))$ and S data simultaneously by means of the nonlinear least-squares method (Fig. 5, bold curve) indicated that Eqs. (18), (19) and (20) reproduced the data well. Overall, the $K_{eq}^{S}(T)$ value for CH_2F_2 in a-seawater can be represented by

$$\ln(K_H(T)/K_{eq}^{S}(T)) = [-0.2261 + 0.5176\times(T/100)] \times S^{0.5} + [0.0362 - 0.1046\times(T/100)] \times S. \quad (21)$$

Plots of k_{s1} and k_{s2} against temperature (Fig. S10) indicate that the absolute values of k_{s1} are much larger than those of k_{s2}; that is, $\ln(K_H(T)/K_{eq}^{S}(T))$ depends predominantly on $S^{0.5}$ rather than on S. The reason for this salting-out effect of CH_2F_2 solubility in a-seawater is not clear.

In Eq. (21), $K_H(T)$ is represented by Eq. (13), as described in Sect. 3.1. Therefore $K_{eq}^{S}(T)$ is represented by Eq. (22):.

$$\ln(K_{eq}^{S}(T)) = -49.7122 + 77.7018\times(100/T) + 19.1379\times\ln(T/100) + [-0.2261 + 0.5176\times(T/100)] \times S^{0.5} + [0.0362 - 0.1046\times(T/100)] \times S \quad (22)$$

The values calculated with Eq. (22) are indicated by the bold curves in Fig. 4 and are listed in Table 3. Equation (22) reproduced the experimentally determined values of $K_H(T)$ and $K_{eq}^{S}(T)$ within the uncertainty of these experimental runs.

3.3 Dissolution of CH_2F_2 in the ocean mixed layer and its influence on estimates of CH_2F_2 emissions

The solubility of CH_2F_2 in a-seawater can be represented as a function of temperature and salinity relevant to the ocean (Eq. (22)). Monthly averaged equilibrium fractionation values of CH_2F_2 between the atmosphere and the ocean (R_m in Gg

Atmos. Chem. Phys. Discuss., doi:10.5194/acp-2017-58, 2017
Manuscript under review for journal Atmos. Chem. Phys.
Discussion started: 8 February 2017

Atmospheric Chemistry and Physics Discussions

patm^{-1}, where patm is 10^{-12} atm) in that the ocean mixed layer is at solubility equilibrium with the atmosphere is estimated as follows. If we divide the global ocean into 0.25°×0.25° grids, R_m can be estimated from the sum of the equilibrium fractionation values from the gridded cells:

$$R_m = \frac{m_{d,m}}{P_a} = Q \sum_{i=-360}^{i=360} \sum_{j=-720}^{j=720} K_{eq}^{S}(T) d_{i,j,m} A_{i,j,m} \quad (23)$$

where $m_{d,m}$, in Gg, is the amount of CH_2F_2 dissolved in the ocean mixed layer; p_a, in 10^{-12} atm, is the CH_2F_2 partial pressure in the air; $d_{i,j,m}$ is the monthly mean depth, in m, of the ocean mixed layer in each grid cell; $A_{i,j,m}$ is the oceanic area, in m^2, in each grid cell; Q is a conversion factor (with a value of 52); m is the month index; and i and j are the latitude and longitude indices. We obtained monthly 0.25°×0.25° gridded sea surface temperatures and sea surface salinities from WOA V2 2013 data collected at 10 m depth from 2005 to 2012 (https://www.nodc.noaa.gov/OC5/woa13/woa13data.html; Boyer et al., 2013) and monthly 2° × 2° gridded mean depths of the ocean mixed layer from Mixed layer depth climatology and other related ocean variables in temperature with a fixed threshold criterion (0.2°C) (http://www.ifremer.fr/cerweb/deboyer/mld/Surface_Mixed_Layer_Depth.php; de Boyer Montégut et al., 2004). Values of $A_{i,j,m}$ were estimated to be equal to the area of each grid cell in which both gridded data were unmasked.

Figure 6 shows the R_m values for the global and the semi-hemispheric atmosphere. Values of R_m for the global atmosphere are between 0.057 and 0.096 Gg patm^{-1}. Because 10^{-12} atm of CH_2F_2 in the global atmosphere corresponds to 9.4 Gg of atmospheric burden of CH_2F_2, 0.6 to 1.0 % of the atmospheric burden resides in the ocean mixed layer when that layer is at solubility equilibrium with the atmosphere. The magnitude of "buffering" of the atmospheric burden of CH_2F_2 by the additional CH_2F_2 in ocean surface waters is therefore realistically limited to only about 1 % globally. However, such buffering would be more effective in each lower tropospheric semi-hemisphere of the AGAGE 12-box model, which has been used for a top-down estimate of CH_2F_2 emissions. The right vertical axis of Fig. 6 represents the residence ratios of CH_2F_2 dissolved in the ocean mixed layer for each lower tropospheric semi-hemispheric atmosphere of the AGAGE 12-box model. The residence ratios were calculated on the assumption that 10^{-12} atm of CH_2F_2 corresponds to 1.2 Gg of atmospheric burden of CH_2F_2 in each lower tropospheric semi-hemisphere. As seen in Figure 6, in the southern semi-hemispheric lower troposphere (30° S–90° S), at least 5 % of the atmospheric burden of CH_2F_2 would reside in the ocean mixed layer in the winter, and the annual variance of the CH_2F_2 residence ratio would be 4%. In the Southern Hemisphere, CH_2F_2 emission rates are much lower than in the Northern Hemisphere. Hence, dissolution of CH_2F_2 in the ocean, even if dissolution is reversible, may influence estimates of CH_2F_2 emissions derived from long-term observational data on atmospheric concentrations of CH_2F_2; in particular, consideration of dissolution of CH_2F_2 in the ocean may affect estimates of CH_2F_2 emissions in the Southern Hemisphere and their seasonal variability.

4 Conclusion

The solubility of CH_2F_2 in aqueous salt solutions relevant to seawater can be represented as a function of temperature and salinity, as shown in Eq. (22). The relationship between CH_2F_2 solubility and the salinity of the artificial seawater was found to be unusual in that the excessive free energy for dissolution depended predominantly on the 0.5 power of salinity. By using the solubility of CH_2F_2 determined in this study, the magnitude of buffering of the atmospheric burden of CH_2F_2 by the additional CH_2F_2 in ocean surface waters is estimated to be realistically limited to only about 1 % globally; however, in a southern semi-hemispheric lower troposphere (30° S–90° S) of the AGAGE 12-box model, the atmospheric burden of CH_2F_2 is estimated to reside in the ocean mixed layer by at least 5 % in the winter and by 1 % in the summer. Hence, it may be necessary that dissolution of CH_2F_2 in the ocean be taken into consideration to derive CH_2F_2 emissions in the Southern Hemisphere and their seasonal variability from long-term observational data on atmospheric concentrations of CH_2F_2.

Supplement link

Supporting information is attached.

Competing interests

The authors declare that they have no conflict of interest.

References

Anderson, G. K.: A thermodynamic study of the (difluoromethane + water) system, J. Chem. Thermodynamics, 43, 1331-1335, doi:10.1016/j.jct.2011.03.020, 2011.

Boyer, T.P., Antonov, J. I., Baranova, O. K., Coleman, C., Garcia, H. E., Grodsky, A., Johnson, D. R., Locarnini, R. A., Mishonov, A. V., O'Brien, T. D., Paver, C. R., Reagan, J. R., Seidov, D., Smolyar, I. V. and Zweng, M. M.: World Ocean Database 2013, NOAA Atlas NESDIS 72, S. Levitus, Ed., A. Mishonov, Technical Ed.; Silver Spring, MD, 209 pp., 2013. http://doi.org/10.7289/V5NZ85MT.

Brockbank, S. A., Russon, J. L., Giles, N. F., Rowley, R. L., and Wilding, W. V.: Infinite dilution activity coefficients and Henry's law constants of compounds in water using the inert gas stripping method, Fluid Phase Equil., 348, 45-51, doi:10.1016/j.fluid.2013.03.023, 2013.

Carpenter, L. J., Reimann (Lead Authors), S., Burkholder, J. B., Clerbaux, C., Hall, B. D., Hossaini, R., Laube, J. C., and Yvon-Lewis, S. A.: Ozone-Depleting Substances (ODSs) and Other Gases of Interest to the Montreal Protocol, Chapter 1, in Scientific Assessment of Ozone Depletion: 2014, Global Ozone Research and Monitoring Project, 55, World Meteorological Organization, Geneva, Switzerland, 2014.

Clarke, E. C. W. and Glew, D. N.: Evaluation of thermodynamic functions from equilibrium constants. Trans. Faraday Soc., 134, 539-547, doi:10.1039/TF9666200539, 1965.

Clegg, S. L. and Whitfield, M.: Activity coefficients in natural waters, Chapter 6, in Pitzer, K. S. (Ed.), Activity coefficients in electrolyte solutions, 2nd ed. CRC Press, Boca Raton, FL, pp. 279-434, 1991.

Clever, H.L., Battino, R., Clever, H.L., Jaselskis, B., Clever, H.L., Yampol'skii, Y.P., Jaselskis, B., Scharlin, and P., Young, C.L.: IUPAC-NIST Solubility Data Series. 80. Gaseous fluorides of boron, nitrogen, sulfur, carbon, and silicon and solid xenon fluorides in all solvents. J. Phys. Chem. Ref. Data, 34, 201-438, doi:10.1063/1.1794762, 2005.

Cunnold, D. M., Fraser, P. J., Weiss, R. F., Prinn, R. G., Simmonds, P. G., Miller, B. R., Alyea, F. N., and Crawford, A. J.: global trends and annual releases of CCl_3F and CCl_2F_2 estimated from ALE/GAGE and other measurements from July 1978 to June 1991. J. Geophys. Res., 99, 1107-1126, doi: 10.1029/93JD02715, 1994.

de Boyer Montégut, C., Madec, G., Fischer, A. S., Lazar, A., Iudicone, D.: Mixed layer depth over the global ocean: an examination of profile data and a profile-based climatology. J. Geophys. Res., 109, C12003, doi:10.1029/2004JC002378, 2004.

Ettre, L., Welter, C., Kolb, B.: Determination of gas-liquid partition coefficients by automatic equilibrium headspace-gas chromatography utilizing the phase ratio variation method. Chromatographia, 35, 73-84, doi:10.1007/BF02278560, 1993.

Hilal, S. H., Ayyampalayam, S. N. and Carreira, L. A.: Air-liquid partition coefficient for a diverse set of organic compounds: Henry's law constant in water and hexadecane. Environ. Sci. Technol., 42, 9231-9236, doi:10.1021/es8005783, 2008.

IPCC, 2013: Climate change 2013: the physical science basis. Contribution of Working group I to the fifth assessment report of the Intergovernmental panel on climate change [Stocker, T. F., Qin, D., Plattner, G.-K., Tignor, M., Allen, S. K., Boschung, J., Nauels, A., Xia, Y. Bex V. and Midgley, P. M. (eds.)], Cambridge University Press, Cambridge, United Kingdom and New York, NY, USA, 1535 pp.

Krummen, M., Gruber, D., and Gmehling, J.: Measurement of activity coefficients at infinite dilution in solvent mixtures using the dilutor technique. Ind. Eng. Chem. Res., 39, 2114-2123, doi:10.1021/ie990830p, 2000.

Kutsuna, S.: Determination of rate constants for aqueous reactions of HCFC-123 and HCFC-225ca with OH^- along with Henry's law constants of several HCFCs. Int. J. Chem. Kinet., 45, 440-451, doi:10.1002/kin.20780, 2013.

Kutsuna, S., and Hori, H.: Experimental determination of Henry's law constant of perfluorooctanoic acid (PFOA) at 298K by means of an inert-gas stripping method with a helical plate, Atmos. Environ., 42, 8883-8892, doi:10.1016/j.atmosenv.2008.09.008, 2008.

Kühne, R., Ebert, R.-U., and Schüürmann, G.: Prediction of the temperature dependency of Henry's law constant from chemical structure, Environ. Sci. Technol., 39, 6705–6711, doi:10.1021/es050527h, 2005.

Lunt, M.F., Rigby, M., Ganesan, A.L., Manning, A.J., Prinn, R.G., O'Doherty, S., Mühle, J., Harth, C.M., Salameh, P.K., Arnold, T., Weiss, R.F., Saito, T., Yokouchi, Y., Krummel, P.B., Steele, L.P., Fraser, P.J., Li, S., Park, S., Reimann, S., Vollmer, M.K., Lunder, C., Hermansen, O., Schmidbauer, N., Maione, M., Arduini, J., Young, D., Simmonds, P.G.:

Reconciling reported and unreported HFC emissions with atmospheric observations. Proceedings of the National Academy of Sciences 112, 5927-5931, doi: 10.1073/pnas.1420247112, 2015.

Maaβen, S., 1995, Experimentelle Bestimmung und Korrelierung von Verteilungskoeffizienten in verdünnten Lösungen, Ph.D. thesis, Technische Universität Berlin, Germany.

Mackay, D., Shiu, W. Y., and Sutherland, R. P.: Determination of air-water Henry's law constants for hydrophobic pollutants, Environ. Sci. Technol., 13, 333-337, doi:10.1021/es60151a012, 1979.

Miguel, A. A. F., Ferreira, A. G. M., and Fonseca, I. M. A.: Solubilities of some new refrigerants in water. Fluid Phase Equil. 173, 97-107, doi:10.1016/S0378-3812(00)00390-3, 2000.

Montzka, S. A., McFarland, M., Andersen, S. O., Miller, B. R., Fahey, D. W., Hall, B. D., Hu, L., Siso, C., and Elkins, J. W.: Recent trends in global emissions of hydrochlorofluorocarbons and hydrofluorocarbons: reflecting on the 2007 Adjustments to the Montreal Protocol. J. Phys. Chem. A, 119, 4439-4449, doi:10.1021/jp5097376, 2015.

O'Doherty, S., Rigby, M., Mühle, J., Ivy, D.J., Miller, B.R., Young, D., Simmonds, P.G., Reimann, S., Vollmer, M.K., Krummel, P.B., Fraser, P.J., Steele, L.P., Dunse, B., Salameh, P.K., Harth, C.M., Arnold, T., Weiss, R.F., Kim, J., Park, S., Li, S., Lunder, C., Hermansen, O., Schmidbauer, N., Zhou, L.X., Yao, B., Wang, R.H.J., Manning, A.J., and Prinn, R.G.: Global emissions of HFC-143a (CH_3CF_3) and HFC-32 (CH_2F_2) from in situ and air archive atmospheric observations. Atmos. Chem. Phys. 14, 9249-9258, doi: 10.5194/acp-14-9249-2014, 2014.

Platford, R.F.: The activity coefficient of sodium chloride in seawater. J. Marine Res., 23, 55-62, 1965.

Prinn, R.G., Weiss, R.F., Fraser, P.J., Simmonds, P.G., Cunnold, D.M., Alyea, F.N., O'Doherty, S., Salameh, P., Miller, B.R., Huang, J., Wang, R.H.J., Hartley, D.E., Harth, C., Steele, L.P., Sturrock, G., Midgley, P.M., McCulloch, A.: A history of chemically and radiatively important gases in air deduced from ALE/GAGE/AGAGE. J. Geophys. Res.-Atmos., 105, 17751-17792, doi:10/1029/2000JD900141, 2000. Website: http://agage.mit.edu

Reichl, A., 1995, Messung und Korrelierung von Gaslöslichkeiten halogenierter ohlenwasserstoffe, Ph.D. thesis, Technische Universität Berlin, Germany.

Rigby, M., Prinn, R. G., O'Doherty, S., Montzka, S. A., McCulloch, A., Harth, C. M., Műhle, J. Salameh, P. K., Weiss, R. F., Young, D., Simmonds, P. G., Hall, B. D., Dutton, G. S., Nance, D., Mondeel, D. J., Elkins, J. W., Krummel, P. B., Steele, L. P., and Fraser, P. J.: Re-evaluation of the lifetimes of the major CFCs and CH_3CCl_3 using atmospheric trends, Atmos. Chem. Phys., 13, 2691-2702, doi: 10.5194/acp-13-2691-2013, 2013.

Sander, R.: Compilation of Henry's law constants (version 4.0) for water as solvent, Atmos. Chem. Phys., 15, 4399-4981, doi:10.5194/acp-15-4399-2015, 2015.

Weiss, R. F.: The solubility of nitrogen, oxygen and argon in water and seawater, Deep-Sea Res., 17, 721-735, doi:10.106/0011-7471(70)90037-9, 1970.

Weiss, R. F. and Price, B. A.: Nitrous oxide solubility in water and seawater, Marine Chem., 8, 347-359, doi:10.1016/0304-4203(80)90024-9, 1980.

Yaws, C.L., Yang, H.-C., 1992. Chapter 11, Henry's law constant for compound in water, in: Yaws, C.L. (Ed.), Thermodynamic and Physical Property Data. Gulf Publishing, Houston, TX, pp. 181-206.

Yvon-Lewis, S.A. and Butler, J.H.: Effect of oceanic uptake on atmospheric lifetimes of selected trace gases. J. Geophys. Res.-Atmos., 107, 4414, doi:10.1029/2001JD001267, 2002.

Atmos. Chem. Phys. Discuss., doi:10.5194/acp-2017-58, 2017
Manuscript under review for journal Atmos. Chem. Phys.
Discussion started: 8 February 2017

Atmospheric Chemistry and Physics Discussions

Table 1. The average of values of $F/(k_1RTV)$ obtained for V value of 0.350 dm^3 and 0.300 dm^3 and the $K_H(T)$ value derived from Eq. (13) at each temperature. N represents number of experimental runs for the average.

T (K)	F / (k_1RTV)				$K_H(T)$ (M atm^{-1})
	V = 0.350		V = 0.300		
	average [a]	N	average [a]	N	From Eq. (13) [b]
276.15	0.119 ± 0.006	21	0.117 ± 0.006	11	0.118 ± 0.003
278.35	0.107 ± 0.005	18	0.110 ± 0.005	14	0.108 ± 0.002
283.65	0.093 ± 0.003	27	0.092 ± 0.001	5	0.094 ± 0.002
288.65	0.082 ± 0.006	41	0.084 ± 0.006	12	0.082 ± 0.002
293.45	0.071 ± 0.001	15	0.071 ± 0.001	5	0.072 ± 0.002
298.15	0.064 ± 0.002	30	0.067 ± 0.005	12	0.064 ± 0.002
303.05	0.057 ± 0.003	16	0.056 ± 0.005	4	0.058 ± 0.002
307.95	0.051 ± 0.001	12	0.054 ± 0.004	10	0.052 ± 0.002
312.65	0.046 ± 0.001	13	0.047 ± 0.001	4	0.048 ± 0.001

a. Errors are 2σ for the average only.; b. Errors are 95% confidence level for the regression only.

Table 2. K_H^{298} and ΔH_{sol} values derived from Eqs. (11′) and (13), along with literature data for K_H^{298} and ΔH_{sol}

K_H^{298} (M atm^{-1})	ΔH_{sol} (kJ mol^{-1})	
0.064	−17.2	This work
0.070	−20	Maaβen (1995)[a]
0.070	−19	Reichl (1995)[a]
0.069[c]	−20.6	Anderson (2011)
0.085		Hilal et al. (2008)[a]
	−18.6, −19.7	Kühne et al. (2005)[a]
0.087		Yaws (1999)[a]
0.087		Yaws and Yang (1992)[a]
0.030	−27.2	Miguel et al. (2000)[b]

[a] Reviewed by Sander (2015); [b] Reviewed by Clever et al. (2005)

[c] The value was obtained by extrapolation of the data reported at 284.15-296.15 K (Supplementary data in Anderson (2011)) with respect to the van't Hoff equation.

Atmos. Chem. Phys. Discuss., doi:10.5194/acp-2017-58, 2017
Manuscript under review for journal Atmos. Chem. Phys.
Discussion started: 8 February 2017

Atmospheric Chemistry and Physics Discussions

Table 3. The average of values of $F/(k_1RTV)$ obtained for V value of 0.350 dm^3 and the $K_{eq}^S(T)$ value derived from Eq. (22) at each salinity and temperature. N represents number of experimental runs for the average.

T (K)	K_{eq}^S (M atm^{-1})								
	salinity, 4.452 ‰			salinity, 8.921 ‰			salinity, 21.520 ‰		
	average [a]	N	Eq. (22)	average [a]	N	Eq. (22)	average [a]	N	Eq. (22)
276.15	0.108 ± 0.006	8	0.108	0.103 ± 0.006	21	0.104	0.095 ± 0.006	20	0.095
278.35	0.099 ± 0.004	12	0.099	0.095 ± 0.006	26	0.095	0.087 ± 0.005	22	0.087
283.65	0.086 ± 0.003	9	0.085	0.083 ± 0.007	24	0.082	0.075 ± 0.004	15	0.076
288.65	0.075 ± 0.004	12	0.074	0.072 ± 0.005	33	0.071	0.066 ± 0.004	20	0.066
293.45	0.065 ± 0.002	10	0.065	0.063 ± 0.003	27	0.062	0.058 ± 0.003	14	0.058
298.15	0.058 ± 0.002	13	0.058	0.056 ± 0.004	26	0.056	0.052 ± 0.003	20	0.052
303.05	0.052 ± 0.001	8	0.052	0.049 ± 0.004	14	0.050	0.046 ± 0.003	16	0.046
307.95	0.047 ± 0.002	13	0.047	0.046 ± 0.004	23	0.045	0.042 ± 0.003	16	0.042
312.65	0.042 ± 0.001	7	0.042	0.040 ± 0.003	12	0.041	0.038 ± 0.002	16	0.038

T (K)	K_{eq}^S (M atm^{-1})					
	salinity, 36.074 ‰			salinity, 51.534 ‰		
	average [a]	N	Eq. (22)	average [a]	N	Eq. (22)
276.15	0.088 ± 0.005	21	0.088	0.081 ± 0.003	10	0.082
278.35	0.079 ± 0.006	20	0.081	0.077 ± 0.003	15	0.076
283.65	0.069 ± 0.002	18	0.071	0.067 ± 0.001	9	0.066
288.65	0.062 ± 0.004	19	0.062	0.059 ± 0.002	14	0.058
293.45	0.054 ± 0.002	19	0.055	0.052 ± 0.001	7	0.052
298.15	0.049 ± 0.002	24	0.049	0.047 ± 0.002	15	0.047
303.05	0.044 ± 0.002	16	0.044	0.042 ± 0.001	8	0.042
307.95	0.040 ± 0.002	15	0.040	0.038 ± 0.002	12	0.039
312.65	0.036 ± 0.002	16	0.037	0.036 ± 0.001	7	0.036

a. Errors are 2σ for the average only.

Atmos. Chem. Phys. Discuss., doi:10.5194/acp-2017-58, 2017
Manuscript under review for journal Atmos. Chem. Phys.
Discussion started: 8 February 2017

Atmospheric Chemistry and Physics Discussions

Figure captions

Figure 1. Plots of values of $F/(k_1RTV)$ against F at each temperature for 0.350 dm^3 and 0.300 dm^3 of deionized water.

Figure 2. van't Hoff plot of the K_H values obtained by the IGS method and the PRV-HS method. Bold curve displays the fitting of the data obtained by the IGS method and the PRV-HS method (Eq. (13)). Dashed curves display upper and lower 95% confidence limit of the above fitting by Eq. (12).

Figure 3. Plots of values of $F/(k_1RTV)$ against F at each temperature for 0.350 dm^3 of a-seawater at 36.074‰.

Figure 4. van't Hoff plot of the K_{eq}^S values for a-seawater at each salinity. Dashed curve represents the K_H values by Eq. (13). Bold curves represent the fitting obtained by Eq. (22).

Figure 5. Plots of $\ln(K_H(T)/K_H^S(T))$ vs. salinity in a-seawater at each temperature. Bold curves represent the fitting obtained by Eq. (21).

Figure 6. Plots of monthly averaged equilibrium fractionation of CH_2F_2 between atmosphere and ocean, R_m (Gg $patm^{-1}$) in the global and the hemispheric atmosphere. Right vertical axis represents the residence ratio of CH_2F_2 in the ocean, instead of R_m, for each lower tropospheric semi-hemisphere of the AGAGE 12-box model.

Atmos. Chem. Phys. Discuss., doi:10.5194/acp-2017-58, 2017
Manuscript under review for journal Atmos. Chem. Phys.
Discussion started: 8 February 2017

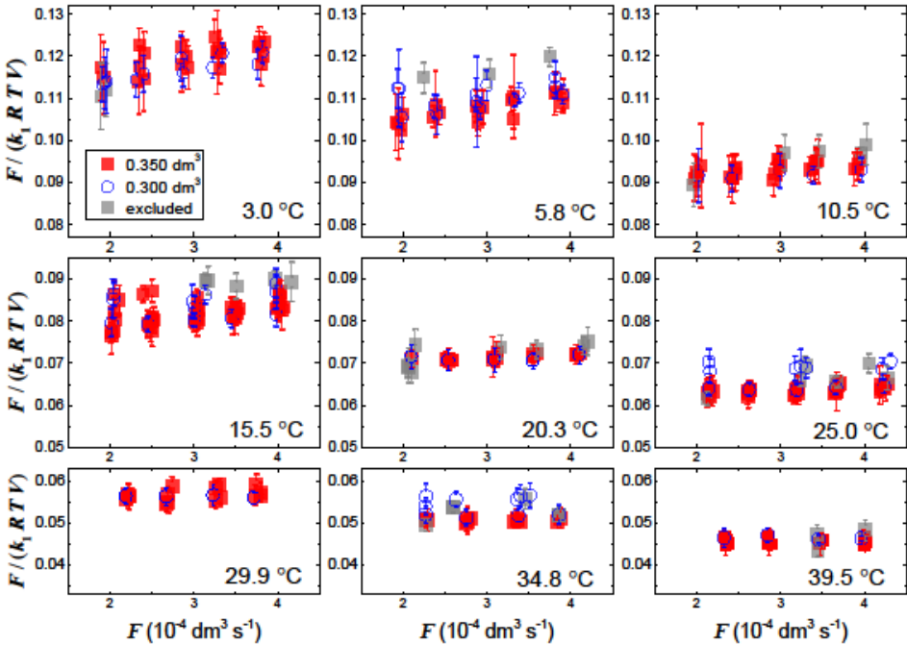

Figure 1. Plots of values of $F/(k_1RTV)$ against F at each temperature for 0.350 dm^3 and 0.300 dm^3 of deionized water. Grey symbols represent the data excluded for calculating the average.

Atmos. Chem. Phys. Discuss., doi:10.5194/acp-2017-58, 2017
Manuscript under review for journal Atmos. Chem. Phys.
Discussion started: 8 February 2017

Atmospheric Chemistry and Physics Discussions

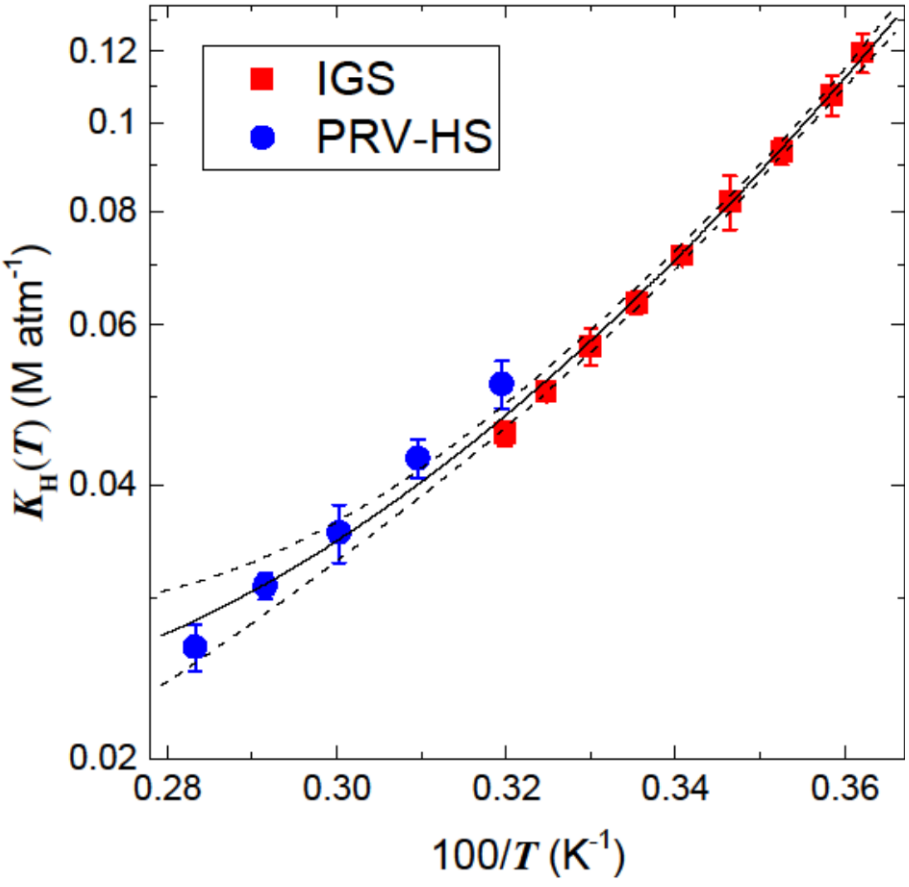

Figure 2. van't Hoff plot of the K_H values obtained by the IGS method and the PRV-HS method. Bold curve displays the fitting of the data obtained by the IGS method and the PRV-HS method (Eq. (13)). Dashed curves display upper and lower 95% confidence limit of the above fitting by Eq. (12).

Atmos. Chem. Phys. Discuss., doi:10.5194/acp-2017-58, 2017
Manuscript under review for journal Atmos. Chem. Phys.
Discussion started: 8 February 2017

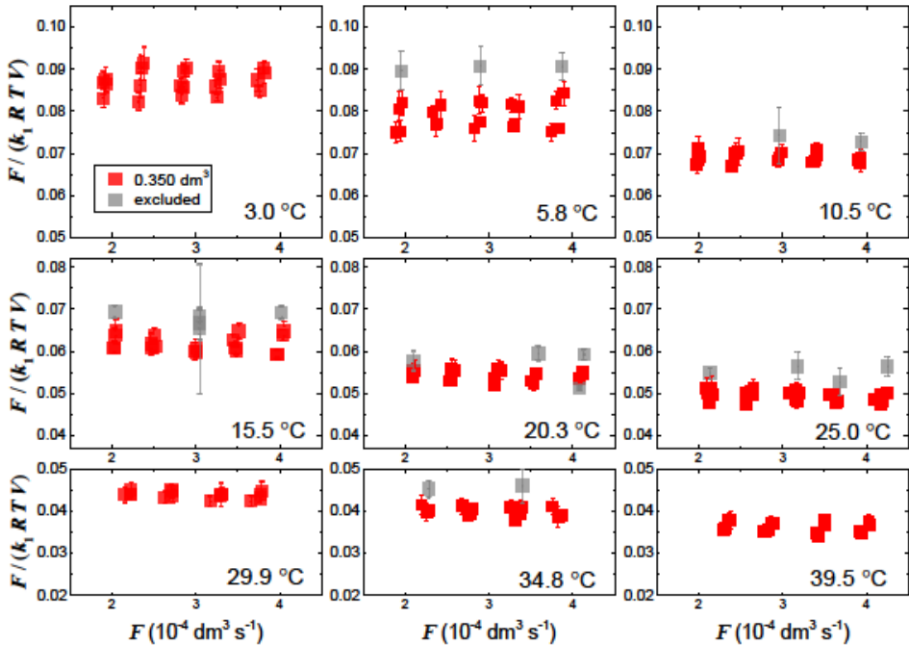

Figure 3. Plots of values of $F/(k_1RTV)$ against F at each temperature for 0.35 dm^3 of a-seawater at 36.074‰. Grey symbols represent the data excluded for calculating the average.

Atmos. Chem. Phys. Discuss., doi:10.5194/acp-2017-58, 2017
Manuscript under review for journal Atmos. Chem. Phys.
Discussion started: 8 February 2017

Atmospheric Chemistry and Physics Discussions

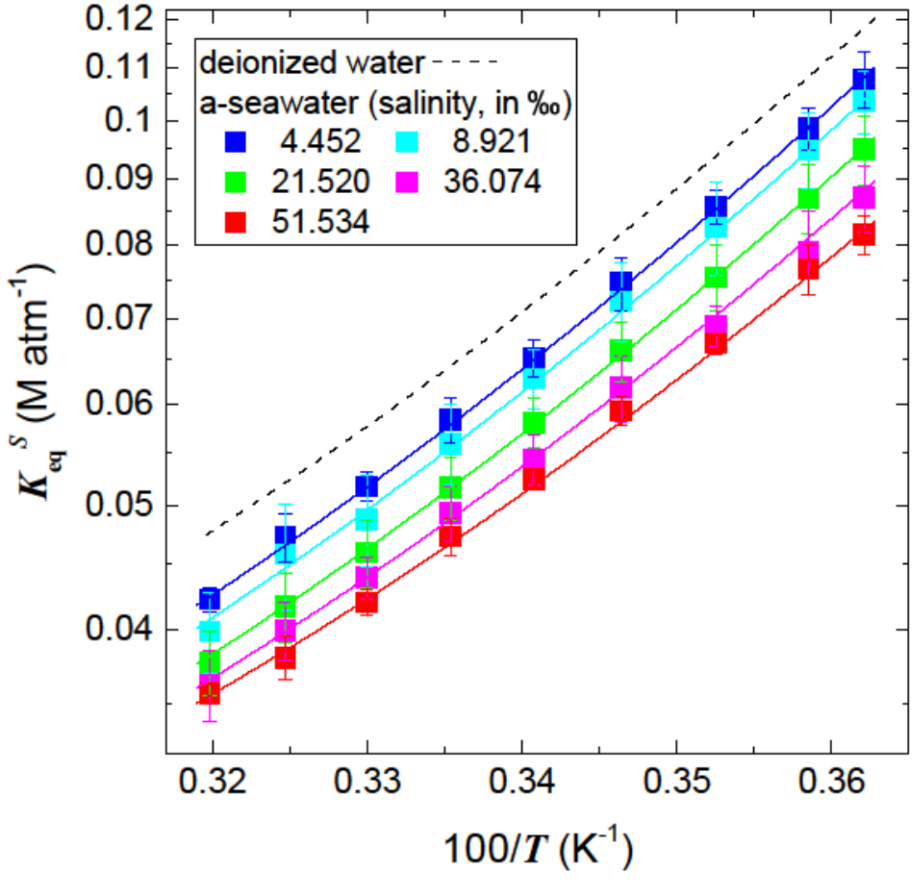

Figure 4. van't Hoff plot of the K_{eq}^{S} values for a-seawater at each salinity. Dashed curve represents the K_H values by Eq. (13). Bold curves represent the fitting obtained by Eq. (22).

Atmos. Chem. Phys. Discuss., doi:10.5194/acp-2017-58, 2017
Manuscript under review for journal Atmos. Chem. Phys.
Discussion started: 8 February 2017

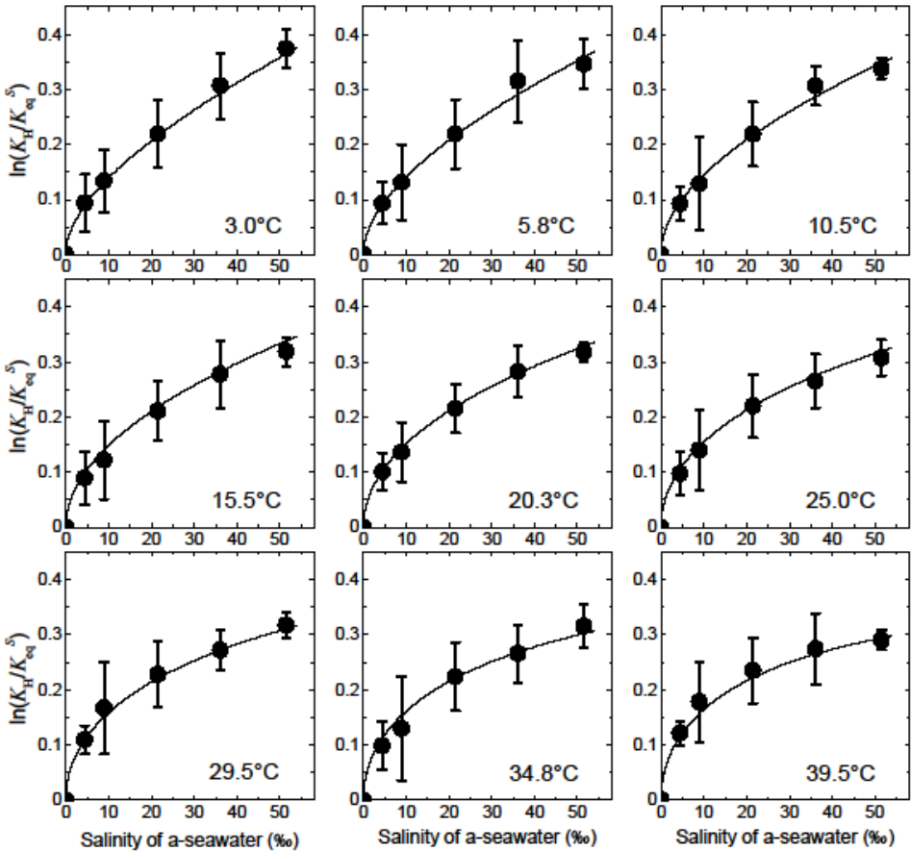

Figure 5. Plots of $\ln(K_H(T)/K_H^S(T))$ vs. salinity in a-seawater at each temperature. Bold curves represent the fitting obtained by Eq. (21).

Atmos. Chem. Phys. Discuss., doi:10.5194/acp-2017-58, 2017
Manuscript under review for journal Atmos. Chem. Phys.
Discussion started: 8 February 2017

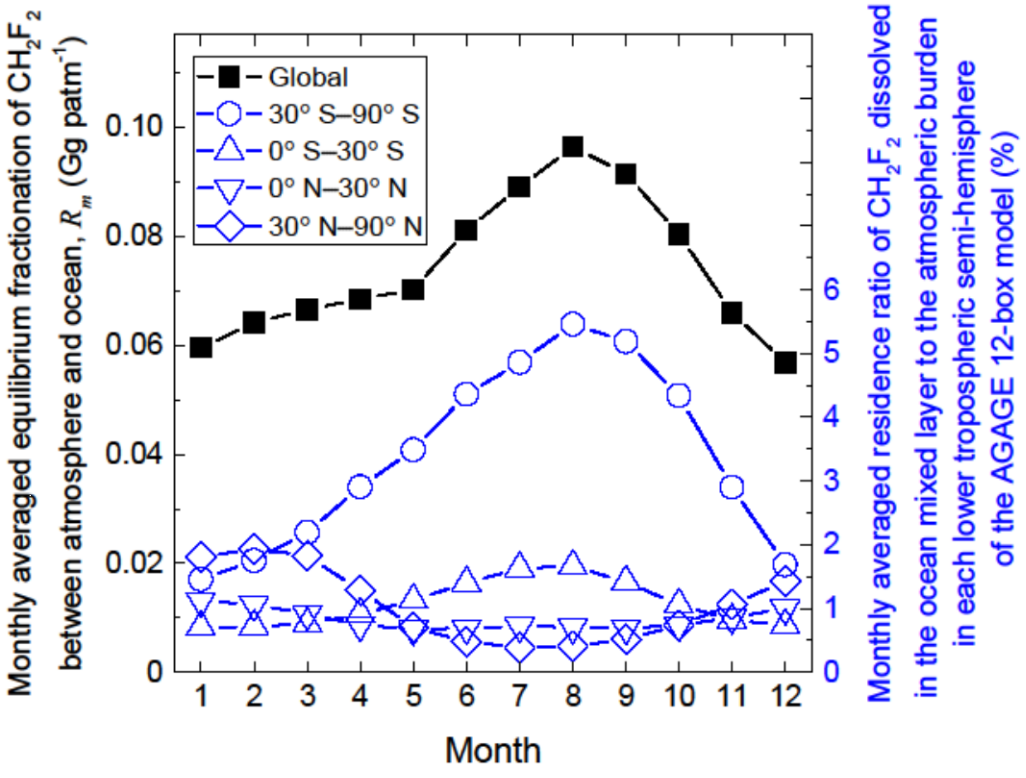

Figure 6. Plots of monthly averaged equilibrium fractionation of CH_2F_2 between atmosphere and ocean, R_m (Gg patm^{-1}) in the global and the hemispheric atmosphere. Right vertical axis represents monthly averaged residence ratio of CH_2F_2 dissolved in the ocean mixed layer to the atmospheric burden for each lower tropospheric semi-hemisphere of the AGAGE 12-box model.